PNAS

Supporting Information for

Global emergence of regional heatwave hotspots outpaces climate model simulations

K. Kornhuber[1,2,3*], S. Bartusek[2,4], R. Seager[2], H. J. Schellnhuber[1*], M. Ting[2,3]
[1]International Institute for Applied Systems Analysis (IIASA), Laxenburg, Austria
[2]Lamont-Doherty Earth Observatory, Columbia University, New York, NY, United States
[3]Columbia Climate School, Columbia University, New York, NY, United States
[4]Department of Earth and Environmental Sciences, Columbia University, NY, United States

*Corresponding Authors:
K. Kornhuber: kornhuber@iiasa.ac.at
H. J Schellnhuber: schellnhuber@iiasa.ac.at

This PDF file includes:

Figures S1 to S12
Tables S1

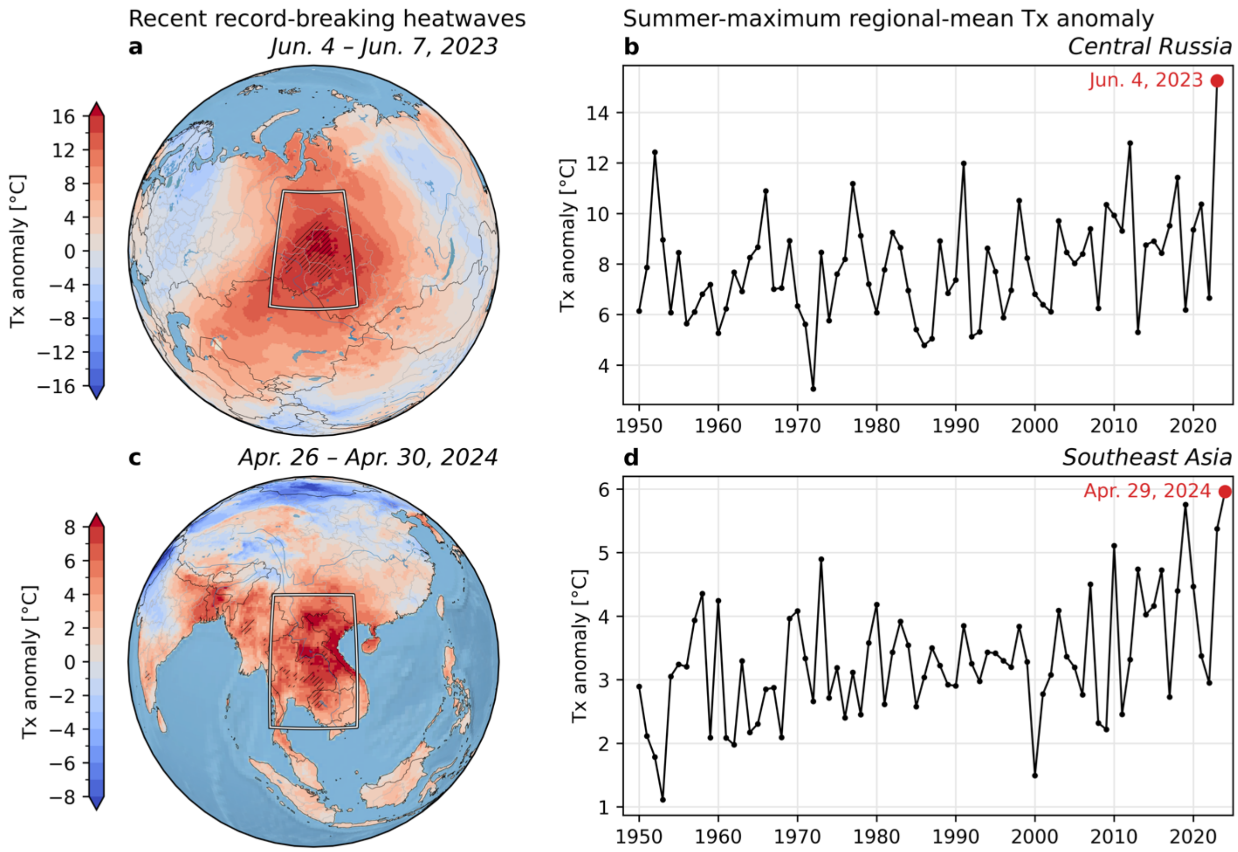

Fig. S1 Daily maximum temperature anomalies during recent record-breaking heatwaves and their temporal context. a 2-meter daily maximum temperature anomaly fields (Tx) of the Northern Hemisphere averaged over the 2023 Siberian heatwave. Regions where values were record-breaking during the indicated time-period are hatched. **b** Time series for the years 1950 - 2023 of the hottest annual Tx anomaly relative to 1981 - 2010 June - August averaged over the region indicated by the box in **a**. The record-breaking values of regional-mean Tx and their dates are highlighted (red dot) in each time series**. c,d** same as **a, b** but for the Southeast Asian Heatwave of 2024.

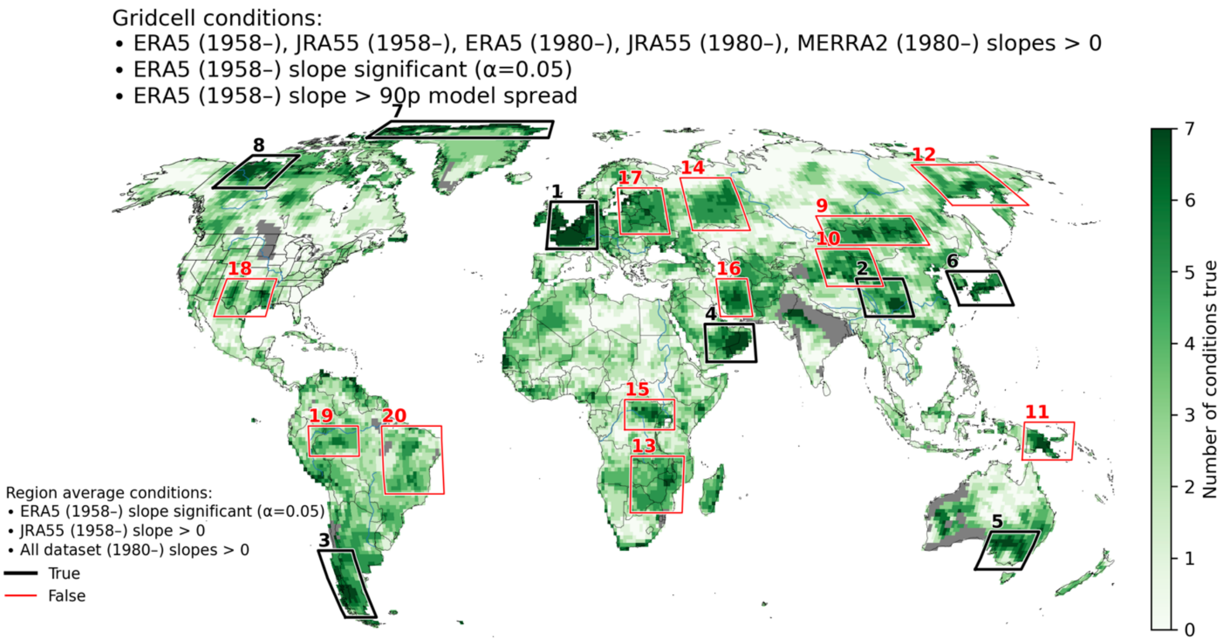

Figure S2 Global map displaying the robustness of regional tail widening and model biases ranked by seven conditions. The conditions are as follows: Conditions 1-5 positive trends across reanalysis datasets and time periods (i. ERA5 (1958-2022), ii. JRA-55 (1958-2022), iii. ERA5 (1980-2022), iv. JRA-55 (1980- 2022), v. MERRA2 (1980 - 2022), vi. significant long-term trend in ERA5 (1958- 2022, $p < 0.05$), which is also vii. stronger in magnitude than the 90th percentile of the model spread (n=49). Regions around areas of interest are outlined above (numbered 1-20). These regions were tested for trends in their regional averages. Regions outlined in black (1, 2, 3, 4, 5, 6, 8), meet the region-average conditions listed on the bottom right, and were therefore selected to be discussed in detail in the main manuscript (Figs. 2, 3, S5). Regions 9-20 fail one of the conditions and are therefore omitted. For completeness, trends and boxplots for all regions are provided in Fig. S3. and Fig. S4.

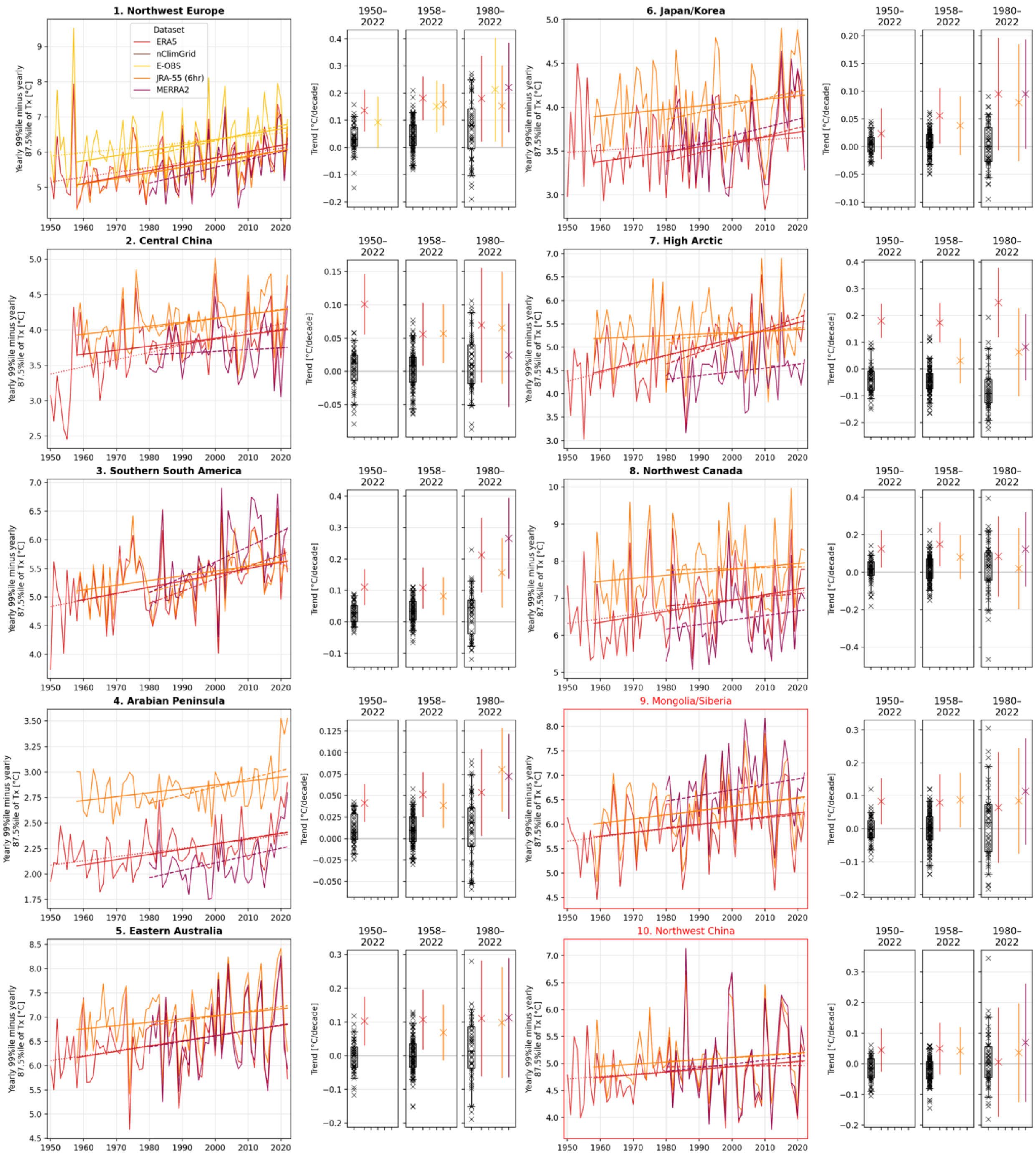

Figure S3 Regional timeseries in tail widening and a comparison of distributions of modelled changes over three different time-periods and corresponding reanalysis and gridded station observation (E-OBS, nClimGrid) datasets. Definitions of regions 1-10 are shown in Fig. S1. An analysis of regions 11-20 is provided in Fig. S3. Regions that do not meet all the selection criteria are outlined in red.

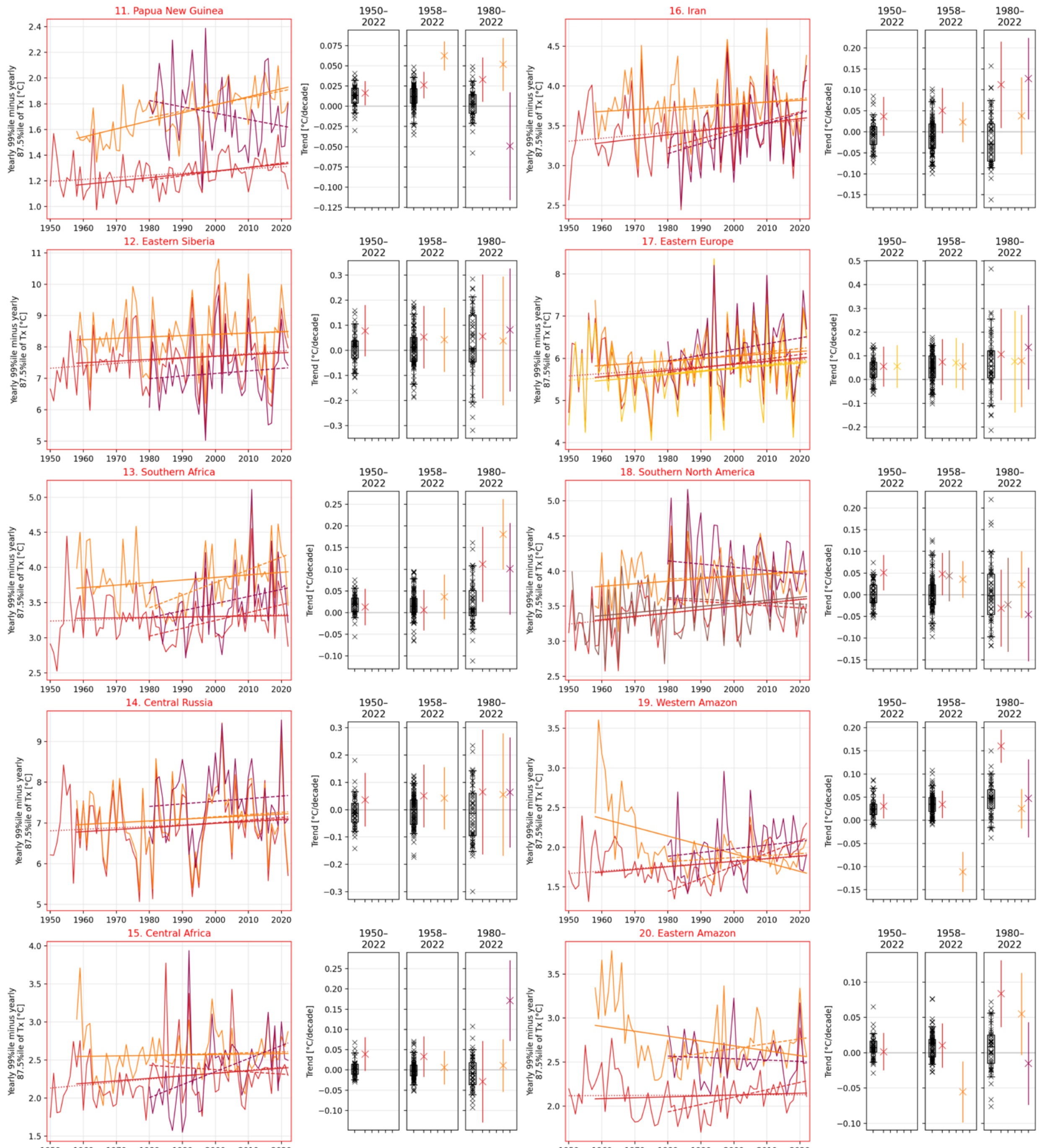

Figure S4 As in S3 but for regions 11-20. Regional timeseries in tail widening and a comparison of distributions of modelled changes over three different time-periods and corresponding reanalysis and gridded station observation (E-OBS, nClimGrid) datasets. Definitions of regions 11-20 are shown in Fig. S1. Regions that do not meet all the selection criteria are outlined in red.

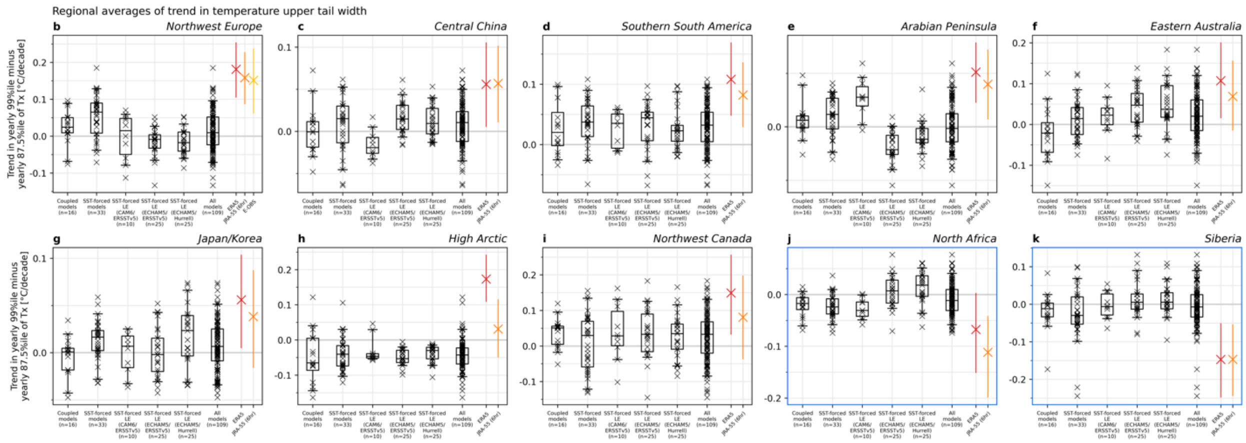

Figure S5 As in Figure 3b–k but including three SST-forced large ensembles (60 members in total) outside of the 49 HighResMIP project model runs provided in Fig. 3 (note that panel letters are kept in line with Fig. 3 to facilitate comparison). In each panel, the first two boxplots and the ERA5 (red), JRA-55 (orange), and E-OBS (yellow) datapoints and uncertainty range are exactly as in Figure 3b–k. The third boxplot displays regional trends from a 10-member ensemble of CAM6 forced by ERSSTv5 historical SSTs, covering 1958–2021. The fourth boxplot shows the same from a 25-member ensemble of ECHAM5 forced by ERSSTv5 covering 1958–2020, and the fifth from a 25-member ensemble of ECHAM5 forced by Hurrell SSTs covering 1958–2020. Note that each of the three extra ensembles shown here do not cover the entire time-period 1958–2022 considered in the main analysis. The sixth boxplot aggregates all 109 model realizations. The ECHAM5 runs (Roeckner et al., 2003) were accessed through the NOAA Facility for Weather and Climate Assessments (FACTS) repository (Murray et al., 2020). The CAM6 runs were accessed through the NCAR Climate Data Gateway thanks to the NCAR Climate Variability & Change Working Group (CVCWG).

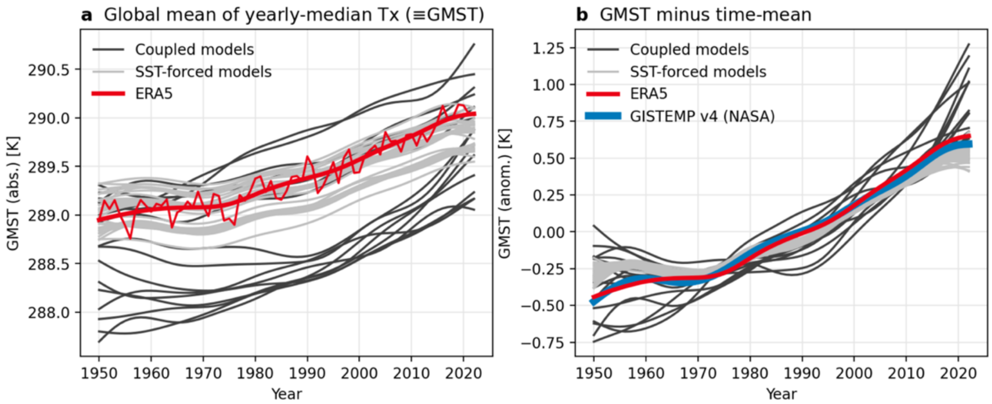

Figure S6 Demonstration of procedure to calculate smoothed global mean near surface temperature (GMST) time series for each model realization and observations, which are used as a trend covariate instead of time in Figs. S3–S4. In **a**, the thin red line shows the global mean (land and ocean points included) of each grid point's annual median Tx. The thick red line shows this time series smoothed by a low-pass filter to retain only variability of frequencies over 10 years (i.e. a 10-yearly cutoff, third-order Butterworth filter, applied forward and backward). In **b**, this smoothed time series is compared against the widely-used NASA GISTEMP v4 GMST time series, subject to the same smoothing (and with the time-means of each over the whole 1950–2022 period removed). Their high similarity justifies the use of Tx data and annual medians to generate the GMST time series. Light and dark gray lines in **a** and **b** show smoothed GMST time series for model data.

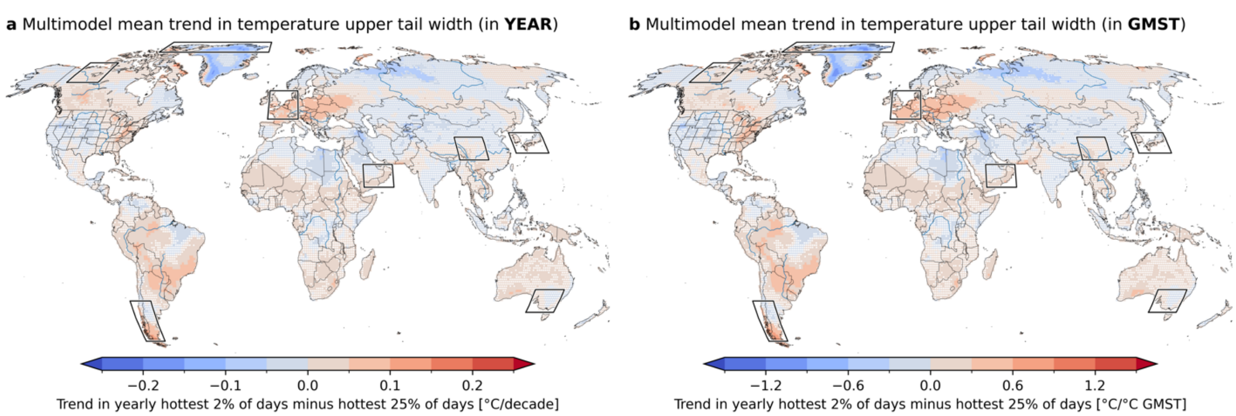

Figure S7 As in Fig. 2a but **a** multi-model mean trend in the changes in the differences of the hottest 2% of annual maximum of daily maximum temperature (Tx) per year with the average of the 25% of days (annual 87.5th percentile of Tx) percentile of the annual maximum temperature at each grid point for years 1950-2022 (as Fig. 2a but for models) **b** the same variables but scaling local temperatures with global mean temperatures.

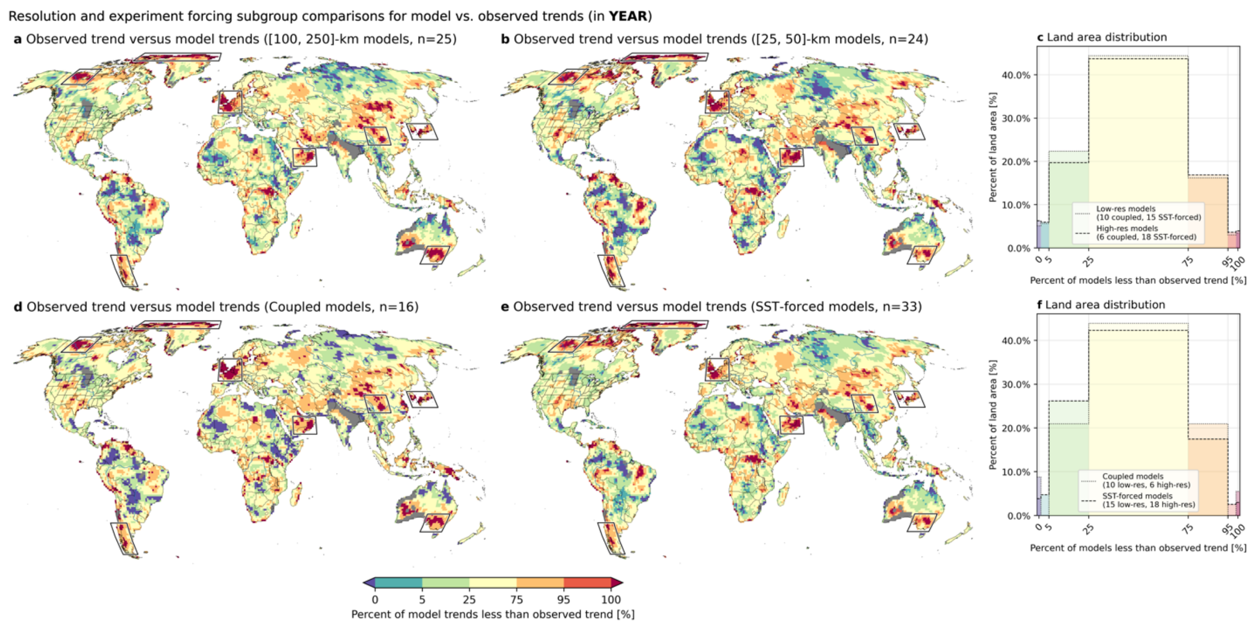

Figure S8 Observed trends in comparison with the models used and distinguished by their resolution and to atmosphere-ocean coupling frameworks a, b, d, e Comparison of observed trends (ERA5) in the widening of the upper quartile (see Fig. 3a) in a range of different model subsets and architectures provided **c, f** Collapsing the maps in **a, b, d, e** into histograms. In **c**, histograms provide estimates of the global distribution of the percentages provided in a and b. Color values match the color map provided in the bottom of the figure comparing models with high (n=25) and low resolution (n=24). A high percentage value for the 25th – 75th percentile signifies a better agreement with trends based on reanalysis, while high values in the lower (upper) percentiles relate to an under (over) estimation of trends in models, on a gridcell-by-gridcell basis. The histograms in **f** show the same for trends over land area based on coupled (n-16) vs. SST-forced experiments (n=33). **d** and **e**, respectively.

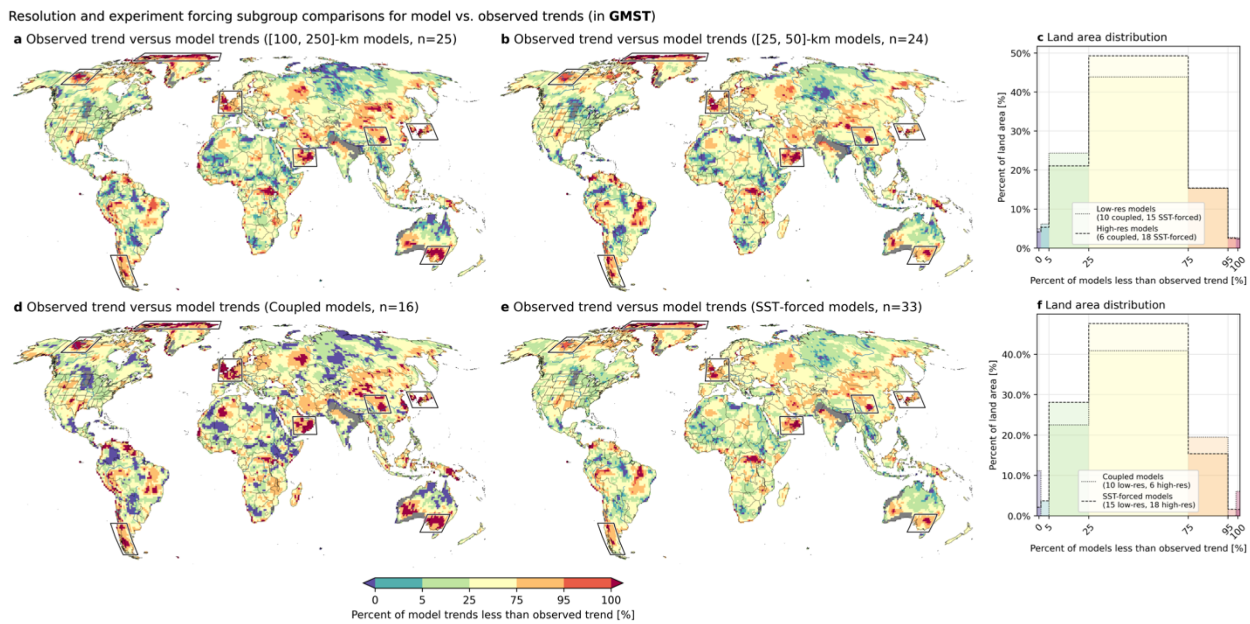

Figure S9 As in Fig. S8 but for GMST level covariate instead of years. a, b, d, e Comparison of observed trends (ERA5) in the widening of the upper quartile (see Fig. 3a) in a range of different model subsets and architectures provided **c, f** Collapsing the maps in **a, b, d, e** into histograms. In **c**, histograms provide estimates of the global distribution of the percentages provided in a and b. Color values match the color map provided in the bottom of the figure comparing models with high (n=25) and low resolution (n=24). A high percentage value for the 25th – 75th percentile signifies a better agreement with trends based on reanalysis, while high values in the lower (upper) percentiles relate to an under (over) estimation of trends in models, on a gridcell-by-gridcell basis. The histograms in **f** show the same for trends over land area based on coupled (n-16) vs. SST-forced (n-33) experiments. **d** and **e**, respectively.

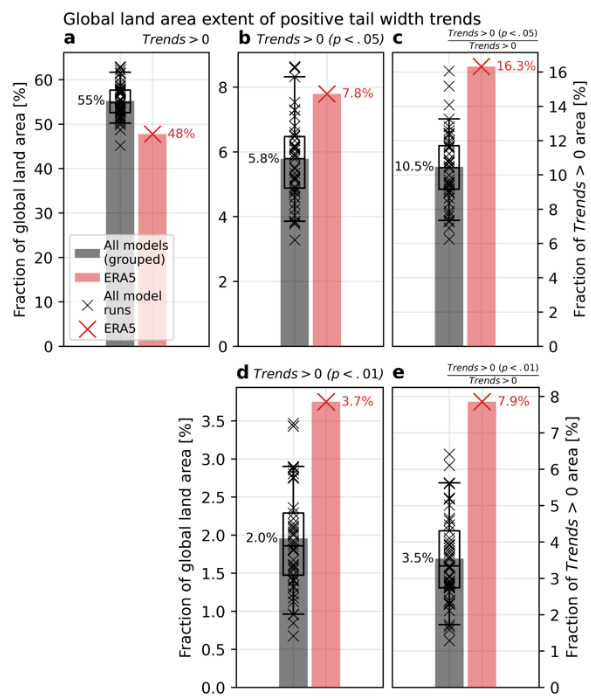

Figure S10 Comparison of global fraction of land area with **a** positive trends, **b** positive trends which are statistically significant ($p < 0.05$) and **c** the fraction of positive trends which are also statistically significant ($p < 0.05$) (right y-axis). **d** Fraction of global land area over which positive trends are significant with a p-value of $p < 0.01$ and **c** the respective fraction compared to all grid points with positive trends (right y-axis).

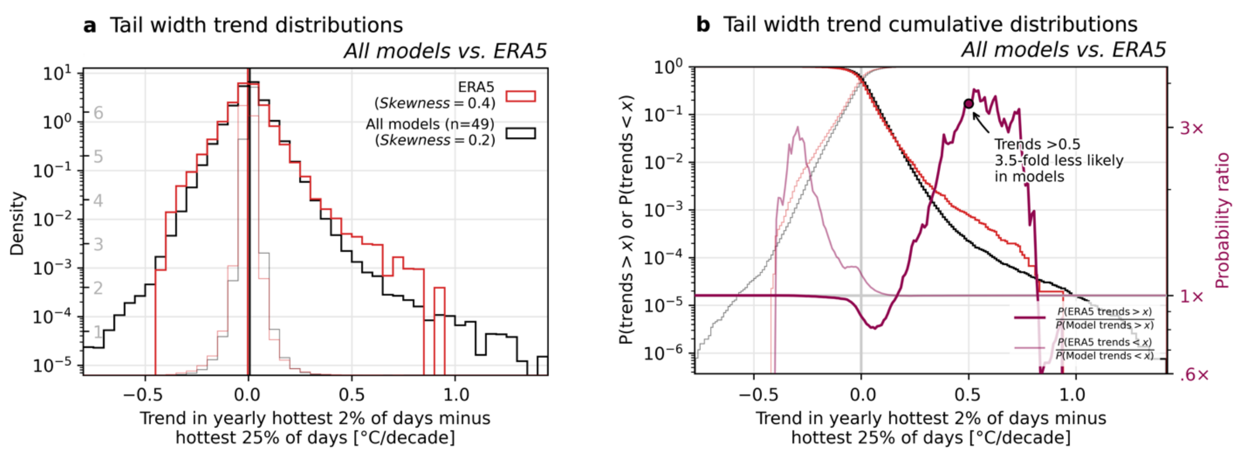

Fig. S11 Alternative depiction of data shown in Fig. 4 providing a histogram of all models combined in **a** and cumulative density distributions in **b** across positive and negative trends instead of providing values for each side of the distribution separately. Trends that exceed 0.5 0.5 °C/decade irrespective of sign are underestimated by a factor of 3.5.

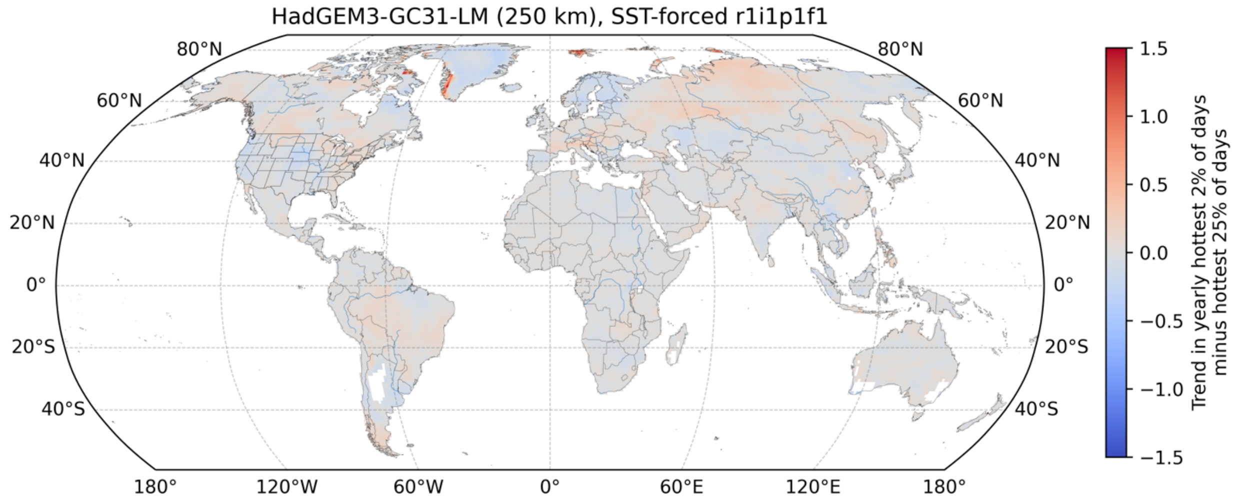

Figure S12 Modelled trends in the hottest 2% compared to the upper 25% for an ensemble member based on HadGEM3. Strong trends are visible in single grid-points in Arctic regions and might be related to modelled singularities linked to assumptions around land and/or sea ice coverage.

Table S1: Model runs and characteristics used in this analysis. Note that some models feature more than one ensemble member.

Institution	**Model**	**Nominal resolution**	**Configuration**	**Number of members**
AS-RCEC	HiRAM-SIT-HR	25 km	SST-forced	1
AS-RCEC	HiRAM-SIT-LR	50 km	SST-forced	1
CAS	FGOALS-f3-L	100 km	SST-forced	1
CNRM-CERFACS	CNRM-CM6-1	250 km	SST-forced	8
CNRM-CERFACS	CNRM-CM6-1	250 km	Coupled	2
CNRM-CERFACS	CNRM-CM6-1-HR	50 km	SST-forced	9
CNRM-CERFACS	CNRM-CM6-1-HR	50 km	Coupled	2
EC-Earth-Consortium	EC-Earth3P	100 km	SST-forced	1
EC-Earth-Consortium	EC-Earth3P	100 km	Coupled	2

EC-Earth-Consortium	EC-Earth3P-HR	50 km	SST-forced	3
EC-Earth-Consortium	EC-Earth3P-HR	50 km	Coupled	3
MIROC	NICAM16-7S	100 km	SST-forced	1
MIROC	NICAM16-8S	50 km	SST-forced	1
MOHC	HadGEM3-GC31-MM	100 km	SST-forced	1
MOHC	HadGEM3-GC31-MM	100 km	Coupled	2
MOHC	HadGEM3-GC31-LL	250 km	Coupled	3
MOHC	HadGEM3-GC31-LM	250 km	SST-forced	1
MOHC	HadGEM3-GC31-HM	50 km	SST-forced	1
MPI-M	MPI-ESM1-2-HR	100 km	SST-forced	1
MPI-M	MPI-ESM1-2-HR	100 km	Coupled	1
MPI-M	MPI-ESM1-2-XR	50 km	Coupled	1
MRI	MRI-AGCM3-2-H	25 km	SST-forced	1
MRI	MRI-AGCM3-2-S	25 km	SST-forced	1
NOAA-GFDL	GFDL-CM4C192	100 km	SST-forced	1